Optimisation of a novel, sloped module, multibody wave energy converter, using an efficient modelling technique

Optimisation of a novel, sloped module, multibody wave energy converter, using an efficient modelling technique

A. Cotten, D. I. M. Forehand

Institute for Energy Systems, School of Engineering, The University of Edinburgh

Abstract

Whilst energy can be efficiently extracted from waves by a device exhibiting sloped motion, sustaining that performance in a deep water environment would conventionally rely on a costly support structure. Introduced herein, the WaveTrain device provides an alternative approach to retain the benefits of sloped motion, using a series of joints and struts to mechanically interconnect a series of sloped modules, each of which houses an internal water column to allow reaction against the surrounding water inertia. With a view to maximal power extraction in a real wave climate, this paper presents an optimisation of key parameters associated with the geometry and mass distribution. This relies upon an efficient hydrodynamic model, whose development is presented, particularly with respect to the use of 'generalised' modes to model hinges, for which a somewhat didactic treatment is given. A genetic algorithm, tailored specifically to handle the discontinuous parameter space and the numerical hydrodynamic model, is then used to identify design criteria that are essential for optimal power extraction. Five necessary but not sufficient criteria are presented, in addition to guidance regarding the remaining parameters, which is used to briefly highlight the potential benefits for the practical engineering design.

Keywords: Generalised modes, heuristic optimisation, hydrodynamic modelling, wave energy converter, WaveTrain

1. Introduction

There exist numerous device concepts for extracting energy from waves, amongst which there are many different operational principles involving various modes of motion [1]. One such concept is that of the IPS Buoy [2]. The IPS Buoy is a heaving point absorber consisting of a hollow vertical tube with a piston inside. The system was designed so that the piston would react against

Email addresses: Alfred.Cotten@ed.ac.uk (A. Cotten), D.Forehand@ed.ac.uk (D. I. M. Forehand)

the inertial water mass inside the tube. The provision of a mass from the Wave Energy Converter (WEC) itself (or from the surrounding water) to act as a reaction mechanism for the Power Take-Off (PTO) system eliminates the need for rigid attachment to the seabed. This then avoids the use of costly support structures and reduces loading on the mooring system. This in turn is a practical requirement for the utilisation of the substantial offshore wave energy resource. The IPS Buoy also has the benefit of requiring no physical end-stops, as the tapered tubing allows water to rush around the piston as it nears its motion limits.

However, for heaving buoys to be well-tuned to the waves in real sea conditions, either a large mass is required to counteract the hydrostatic forces, or an elaborate control system is needed to lengthen the natural period. An alternative solution is provided by tilting the axis of motion towards the horizontal, thus reducing the hydrodynamic stiffness, and lengthening the natural period without a significant increase in the device mass. Combining this operational principle with the aforementioned type of PTO led to the development of the Sloped IPS Buoy [3]. Early work on this device confirmed that constraining the motion of a WEC to an inclined axis can result in very high power absorption over a wide range of frequencies [4]. For deep water deployment, the device must maintain these benefits without the rigid constraint on the axis of motion. Unfortunately, testing of freely-floating versions revealed a collapse of that high and broad power absorption profile [5], as the resulting pitching motion tended to cause dissipation of much of the energy [6]. The WaveTrain concept [7][8] presented herein provides a potential solution to this problem, enabling retention of the good power absorption characteristics, whilst avoiding the need for any kind of rigid connection to the seabed.

The key innovation of the WaveTrain concept is to mechanically interlink multiple sloped buoy modules, so that free motion along the inclined plane is retained, whilst restricting the counterproductive pitch motions (Fig. 1). To this end, rotational joints at each end of the connecting struts enable the exchange of restorative forces between neighbouring sloped modules, which enforces the desired restrictions on the device motions. Those forces are best provided when the struts are perpendicular to the modules. Hence, with each module orientated at its intended inclination angle, the struts are connected so as to form right-angles with the module surfaces when the device is floating in its equilibrium position. The mass distributions are key in ensuring that the intended equilibrium position is achieved. (Evidence of this configuration enabling the prevalence of the intended sloped motion can be found in [7][8].)

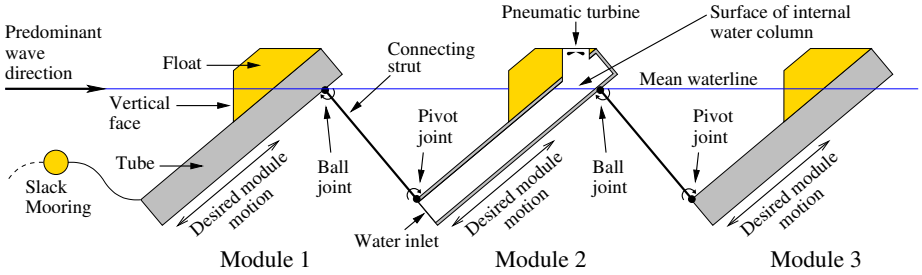

Figure 1: Equilibrium configuration of a three-module WaveTrain device, 'in-plane' view. The modules are arranged in an attenuator configuration (i.e. parallel to the predominant wave direction). The central module is shown with a cutaway view to illustrate the internal water column, enclosed air chamber and pneumatic turbine, all of which are present within each module.

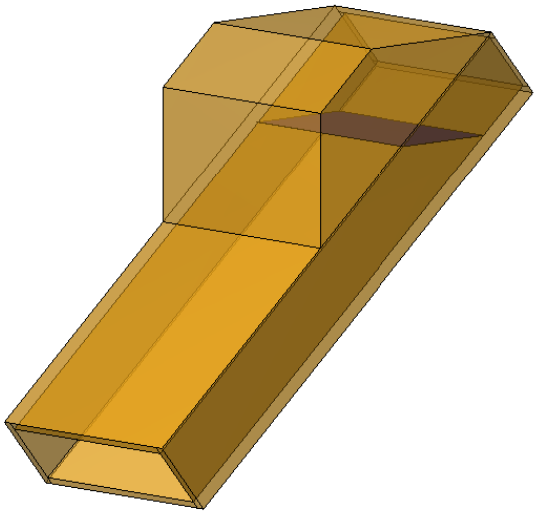

Figure 2: Transparent, isometric drawing of a single module of the WaveTrain device in its equilibrium position, showing the internal free surface.

Though only in-plane motions are desired for power extraction, employing all three rotational degrees of freedom (DoFs) in just the uppermost joints (see the ball joints in Fig. 1) allows some limited out-of-plane motions to alleviate loadings. Conversely, the pivot joints at the bottom of each strut only allow in-plane rotations. Each module incorporates a hollow tubular section, which is open at its bottom end - see the cutaway view of the central module in Fig. 1, along with Fig. 2). The motion of the internal free surface is then used

to force the air above through a pneumatic turbine. These separate PTOs are situated atop each module, and the whole device resembles a series of floating oscillating water column devices, albeit with each wave-activated body acting in unison with its internal water column in order to provide the power extraction. The internal water columns are primarily a means by which to react against the inertial mass of the surrounding water. Each module also utilises a float of lower density material, in order to both provide buoyancy, and present a vertical face to the incoming waves, so that a sufficient surge component of motion can result. The whole device is slack-moored via the front module (see Fig. 1), which allows the WaveTrain to weather-vane towards the predominant wave direction.

Originally developed by Dr. Nicholas Wells, the WaveTrain concept recently underwent physical and numerical model testing as part of Wave Energy Scotland's Novel WEC programme [9]. The key recommendation from that work for driving the concept forward was to optimise the geometric and mass properties of the device, and a time-domain model developed as part of the project was proposed for use in such an optimisation process. Despite this model's success in combining an empirical quadratic drag term with a nonlinear multibody solver and a linear hydrodynamic model, it was also noted that a purely linear model could be sufficient for an optimisation scheme [8]. Disregarding the nonlinearities removes the necessity for a time-domain approach. Instead, all of the device dynamics can be more efficiently accounted for in the frequency-domain, permitting a faster and broader search for optimal design candidates.

In order to construct such a frequency-domain model of the WaveTrain device, an efficient means of representing its motions is required. The motions of a rigid body can be described by a combination of the 6 standard modes (surge, sway, heave, roll, pitch and yaw), whereas deformable (including jointed) bodies require additional, 'generalised' modes of motion to account for the extra DoFs. For example, the three-module WaveTrain device can be viewed as a single rigid body, augmented by extra joint rotations and relative motions of the internal water columns. The 6 standard modes of motion describe the behaviour of the rigid body component, with generalised modes of motion used to describe the hinge deflections, and also the internal water column movements (see Section 4.3.3). In the context of the interaction with waves, generalised modes involve defining additional velocity potentials that can be solved for using the WAMIT software [10]. In particular, jointed systems have been modelled using generalised modes before. However, to the authors' knowledge, the published studies on this topic only present cases with relatively simple geometries and hinge arrangements, with many also providing only brief details of the implementation.

In this paper, an efficient hydrodynamic model of the WaveTrain concept is developed with a view towards device optimisation. Section 2 aims to reveal the gap in the literature regarding the application of generalised modes to complex body shapes with hinges. Section 3 first surveys the possible optimisation approaches, covering gradient-based methods and metaheuristics, before going on to present the most relevant existing studies in which genetic algorithms were employed to optimise wave energy systems. This is then followed by a summary of the latest results regarding the design of sloped wave energy converters. In

section 4, the application of generalised modes to this novel WEC concept is complemented by a somewhat didactic lesson regarding the implementation details. This model is then used within an heuristic optimisation scheme (Section 5), which is tailored to handle a range of physical design constraints and to overcome the difficulties in using the numerical method to compute the objective function that is to be optimised (Section 6). Optimal configurations of the device are explored in Section 7, and guidance on future design is given along with the main conclusions in Section 8.

2. Literature review of the application of generalised modes to jointed bodies

Generalised modes have previously been applied to jointed bodies, including multibody WECs, in order to model their interactions with waves. Examples found in the literature tend to involve simple geometries and mass distributions, often with implementation details kept brief, despite the potential complexity involved in constructing such models.

After introducing the theory and approach for the general case of deformable bodies interacting with linear water waves, Newman [11] presents the case of two identical cuboidal barges, connected by a central, equidistantly located hinge. By also using a symmetric definition of the rotational motions about the hinge, complexity in the inertia and gravitational restoring forces coupling the modes of motion with one another, is minimised. McNatt [12] applies similar, symmetrical definitions of the hinge motions to three cylindrical barges with spherical ends, using equidistantly spaced hinge locations. In that study, symmetry about the plane perpendicular to the length of the ensemble of modules ('lengthwise symmetry') is present. Mathai [13] does likewise for a set of three hinge-connected cuboidal barges. Newman [14] introduces an alternative choice of generalised modes that can be applied to an ensemble of hinge-connected floating bodies, to analyse the vertical motions. Exploiting the lengthwise symmetry of the chain of bodies, symmetric and antisymmetric variants of the generalised modes are presented, enabling a reduction in runtime. This approach of modelling only the vertical hinge motions is also applied to a hinged assembly of semi-submersible structures by Lee and Newman [15], but 'a uniform distribution of mass and stiffness' is assumed to avoid any further complexity introduced by the geometry. Lengthwise symmetry is also present, as is the case in the four other aforementioned studies. Following Newman's approach [14], Li *et al.* [16] apply generalised modes to analyse the vertical motions of the two hinges of the SeaWEED device. That device's modules are asymmetric, lengthwise, which is likely the reason why symmetric and antisymmetric modes are not used. Still, whilst the shape used for the WAMIT mesh is not presented, the device design suggests at relatively simple geometry and hinge layout. A generalised mode is also used by Xu *et al.* [17] to represent the rotational motion about the hinge connecting two floating bodies. The device does not possess symmetry either side of the hinge, but the geometry is nonetheless rather simple, comprising

mainly cylindrical body components, and forming simple rafts either side of the hinge.

3. Literature review of pertinent optimisation studies

Before surveying studies with direct application to WECs, it is useful to briefly review some of the possible optimisation approaches. (See e.g. [18] for a more comprehensive treatment.) Beyond analytically solvable problems, there is often a distinction made between gradient-based and gradient-free algorithms. Fundamentally, gradient-based methods (see e.g. [19]) involve the computation of the gradient in order to direct the search towards a local minimum. Typically, the cost of this computation is proportional to the number of design variables [20], but state-of-the-art adjoint methods (e.g. [21], [22]) can offer the possibility of obtaining the gradient information at a much-reduced computational cost that is almost independent of the number of design variables [23]. The strategic use of multiple starting points can also be used to allow the search for a global optimum using gradient-based methods. Whilst this type of approach can be very efficient, even in the presence of a limited number of non-smooth points (e.g. [24]), the search still requires a predominance of smooth regions within the search space. Problems whose objective-function spaces are more greatly affected by discontinuities and noisy regions, are often better explored using metaheuristic methods, such as genetic algorithms [25]. Metaheuristics form a subset of gradient-free algorithms. Their searches are directed using previous evaluations of the objective function(s) but without explicit computation of the gradient, and are often inspired by elements of the natural world. In many WEC optimisation problems where the objective functions are based on a numerical solver, the search spaces are likely to contain discontinuities and be noisy and complex in shape, making them particularly amenable to metaheuristic algorithms.

Two of the studies mentioned in the previous section which use generalised modes, [16] and [17], also apply their models towards finding optimal characteristics relating to device geometry. Both cases are reliant on an initial assessment of a sufficient batch of designs, which are then used directly to extract the optimal parameters. However, with larger and/or more complex parameter spaces, metaheuristic algorithms, such as those based on evolutionary principles, are often more appropriate. In particular, genetic algorithms (GAs) have been combined with frequency-domain WEC models, in order to optimise device geometry [26][27][28], with the latter two studies simulating the device motions in irregular wave conditions. A multi-objective genetic algorithm has even been applied, to optimise the physical configuration of a wave energy converter [29]. However, to the authors' knowledge, there are currently no published studies that use a genetic algorithm to optimise a WEC whose operational principle requires motion along a slope. Nevertheless, a small number of studies have investigated the impact of the design parameters on the performance of sloped-motion WECs.

Lin [4] used a mechanical rig to restrict the motion of a buoy to a fixed, sloped axis. Of the four inclination angles tested experimentally in monochromatic waves, 45° was selected for further testing due to its broad-banded high efficiencies. Payne *et al.* [30] used a numerical model to investigate the performance of a freely-floating buoy, whose inclined-plane power take-off reacts against water inertia. It was found that the effective mass of this water should be at least as great as the buoy mass, and should be located at least half a cylinder draught below the centre of the cylindrical buoy. The optimal angle in that study was found to be 40° to the horizontal. López *et al.* [31] used a numerical model to conclude that, of the five angles tested (15°, 30°, 45°, 60° and 75°), the highest extracted powers of a rig-constrained, nearshore WEC resulted when the slope angle was 30° to the horizontal, closely followed by 45°.

4. Development of an efficient hydrodynamic model

Frequency-domain models based on linear hydrodynamics tend to overestimate the device motions in larger waves, but can give a good indication of the general dynamics and dominant modes of operation. Further, given the accuracy of a linear model supplemented by a nonlinear term proportional to the square of the velocity [8] in predicting the WaveTrain's mean power absorption, it may be expected that any overestimates in power given by a fully linear model would not significantly affect the relative rankings in performance of different designs.

4.1. Modelling assumptions

Each device considered during this study comprises three modules, as this provides the simplest case that is representative of the complete system dynamics (i.e. it includes a module with neighbours on either side). It is assumed that the interconnecting mechanical struts will have negligible hydrodynamic effect compared to the modules themselves. Thus in determining the device motions, the model needs to account for the connections, but the hydrodynamic interactions need only involve the three modules (including their internal water columns). It is also assumed that these struts will not significantly impact the dynamics through their mass and inertia, so this is also disregarded. Nevertheless, each strut is to be connected from the base of one module, to a position coinciding with the waterline on the underside of the module in front (Fig. 1). Since the device is intended for deep-water deployment, it is assumed that its slack-mooring will have a negligible effect on the dynamics relevant for power absorption. As observed in previous wave tank tests, the chain of WaveTrain modules tends to align itself perpendicular to the incoming wavefronts. Consequently, the model only needs to capture the in-plane dynamics, which means only a single degree of freedom is required to model each joint. Considering also that each module contains an internal body of water, this leads to a 10 DoF model - the 3 in-plane rigid body DoFs (surge, heave and pitch), 4 DoFs due to the four hinges, and 3 DoFs corresponding to the translational motions of the

three internal water columns. As the power take-off system is expected to be small compared to each module, its effect on the device dynamics through its own mass and inertia is not considered. Indeed, the only contribution of each PTO is via a linear damping coefficient, to account for the effects of removing energy from the system.

The complexity of this WEC concept necessitates that some base assumptions are also made about the physical structure of each module. Each comprises a trapezium-shaped float of uniform density, the base of which is attached to the top of a hollowed-out cuboid, which is open to the surrounding water at the bottom, and whose walls are also of uniform density (Fig. 3). These two components are supplemented by a 'point mass', situated at the leftmost edge of the module (see also Fig. 3), whose role is to enable the desired mass distribution with maximal simplicity (primarily to allow satisfaction of Eq. A.1 for a wide range of designs). All of the surfaces are to be flat, and each of the three modules identical in form.

The trapezium shape of the float allows for a range of vertical-float-face heights and positions with minimal model complexity, whilst broadly capturing a shape that is feasible for a practical realisation. Curved surfaces might be preferred in practice to minimise viscous losses, but would entail a more complex geometry description for the optimisation routines, so are not pursued here.

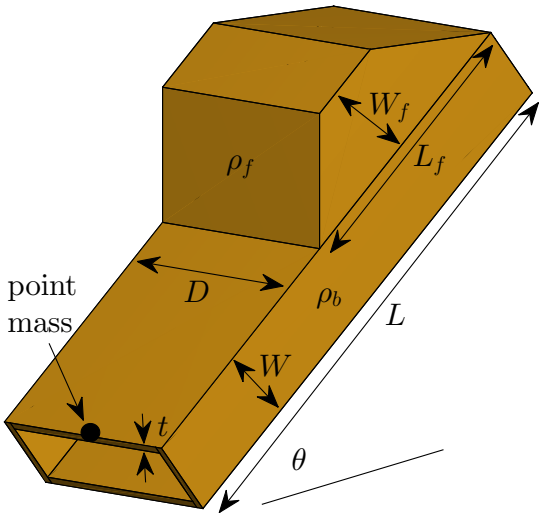

Figure 3: Schematic of a single WaveTrain module, with the defining parameters labelled. θ is the angle between the horizontal plane and the length, L. ρ_f is the density of the float and ρ_b is the density of the tube walls.

4.2. Physical constraints

There are six physical constraints that need to be satisfied to ensure physical feasibility. The physical basis for these is as follows:

1. Each module must freely float with the desired inclination angle when in equilibrium.
2. The device must be statically stable - i.e. it must return to its equilibrium position after a small displacement.
3. The free surface must intersect the body within prescribed limits.
4. The float must be shorter than the main body of the module.
5. The float is shaped as a trapezium in cross-section, so can only be as wide as when the length of the top side of the trapezium tends to zero (i.e. the float is shaped as a triangle when the float width, W_f, takes its upper limit value).

More detail is given regarding these constraints in Appendix A.

4.3. Model construction

WAMIT is used in this study due to its provision of certain required modelling features. See [32] for more detail on the methods described in this section.

4.3.1. General approach and geometry representation

WAMIT's 'higher-order method' is used to represent the variation of the velocity potentials on the bodies as B-splines [32]. Quadratic B-splines are used with a panel size of $0.2L$. Dipole patches are used to efficiently model the thin tube walls, and irregular frequency removal is implemented (see [10]).

4.3.2. Hinges - an applied didactic treatment

Generalised modes can be used to specify types of motion over and above the standard six rigid body modes (surge, sway, heave, roll, pitch and yaw). In order to introduce an additional velocity potential (specifically, a radiation potential) for each new mode of motion, an appropriate 'shape function' [11] (denoted $\mathbf{S}_i(\mathbf{x})$, for mode i) must be specified, which describes the new type of motion as a function of the spatial coordinates. The choice of shape function is not unique, and it is important to derive an appropriate form. Once the shape function is defined, solving for the diffraction potential and all of the radiation potentials then enables computation of the hydrodynamic coefficients (i.e. the added masses A_{ij}, radiation dampings B_{ij}, and excitation forces X_i) using the geometry of the submerged body surfaces, in the same manner as for the rigid body modes. In the case of generalised modes for hinges, the hydrostatic (buoyancy) coefficients, c_{ij}, are also computed automatically by WAMIT (the divergence of the shape functions is zero - see [11]). However, in order to solve the N equations of motion (Eq. 1) for the N degrees of freedom (which include the normal and generalised modes), some special treatment is

first required to compute the inertial and gravitational restoring properties (M_{ij} and C_{ij}), where i or j or both are generalised modes.

$$\sum_{j=1}^{N}[-\omega^2(M_{ij}+A_{ij})+i\omega B_{ij}+c_{ij}+C_{ij}]\xi_j = X_i \text{ for } i=1,...,N \qquad (1)$$

Note that Eq. 1 may contain extra stiffness and damping due to power take-off systems for wave energy applications.

To summarise, there are three quantities with which WAMIT must be provided, that can pose some difficulties in modelling hinges, especially for bodies with a high level of geometric or configurational complexity:

1. Shape functions, $\mathbf{S}_i(\mathbf{x})$
2. Mass/inertia matrix elements, M_{ij}
3. Gravitational restoring force/moment coefficients, C_{ij}

Each of these are treated in turn in Appendix B, outlining a recommended approach whilst emphasising the key conceptual details.

4.3.3. Internal water columns

The WaveTrain device extracts power through the relative motion between each solid module and its internal water column, and so a linear damping force needs to be applied between these two reference frames. Generalised modes can be used for this effect (see [33] for more details), here with a single, translational, 'piston' mode representing each column.

The pitch motions (or any more complex motions) of these internal water column surfaces are neglected for three reasons. Firstly, in wave conditions in which the WaveTrain generates the majority of its energy, the pitch motions of the modules will be small, with translational sloped motion prevalent (see both [7] and [8]). Secondly, for the range of designs considered in this study, and for the wave conditions in which the majority of the energy is contained (see Appendix D for the wave climate used in this study), the width of the internal water columns is small compared to the wavelengths of the incoming waves. Therefore, the likelihood of sloshing inside each WaveTrain module is low within the sea states that contain the majority of the wave energy. Lastly, it is expected that any sloshing modes present within the internal water columns would only cause a negligible change in the air chamber volume, and so would not significantly contribute to power production.

The system is now efficiently modelled using ten modes of motion, equal to the number of degrees of freedom.

5. Construction of optimisation routines

A genetic algorithm is used to optimise the power extraction of the WaveTrain with respect to 6 geometric variables (θ, W, D, L_f, W_f, L) and 2 densities (ρ_b, ρ_f) (Fig. 3), in addition to the linear PTO parameters. Gradient-based

methods are not considered here because the discontinuous nature of the search space would lead to the requirement of a vast number of starting points (see also the analysis of Figures 6 and 7 in section 7). As a result of the numerical solver on which the objective function is based, some amount of noise is also likely to be present in the search space, further discouraging the use of gradient-based algorithms.

The tube wall thickness, t, is held constant (see later). The objective function is based on the hydrodynamic model introduced in Section 4, and is used to compute the average yearly power extraction in a West Shetland Shelf wave climate [27]. In order to reduce the number of optimisation variables involved in the outer loop of the GA, an inner optimisation loop is used to compute the optimal PTO parameters for each candidate design specified by the other eight variables.

5.1. Ensuring physically feasible designs

If supplemented with bounds on the optimisation parameters, the six physical constraints applying to a single WaveTrain module (see Section 4.2) form a closed section of parameter space from which candidate designs must be selected, during the optimisation process. The equality (Eq. A.1) warrants the most attention and should be solved for directly to ensure the equilibrium inclination angle of any physical realisation would be as intended. The point mass can be used to this effect by adjusting the locations of the centre of gravity and centre of buoyancy. Further details are given in Appendix C.

5.2. Objective function

The objective function, f, used in this study is the mean annual power production (Eq. 2) in a West Shetland Shelf wave climate (see Appendix D).

$$f = \frac{1}{|\hat{O}(H_{m0}, T_z)|} \sum_{H_{m0}} \sum_{T_z} \hat{O}(H_{m0}, T_z) \bar{P}(H_{m0}, T_z) \tag{2}$$

where $\hat{O}(H_{m0}, T_z)$ is the annual occurrence (in hours) of the sea state with significant wave height, H_{m0}, and mean zero-crossing period, T_z, and $\bar{P}(H_{m0}, T_z)$ is the corresponding mean power extracted in that sea state. $\bar{P}(H_{m0}, T_z)$ is calculated using superpositions of the relative motion responses of each internal water column lid. This approach is based on the method used by McCabe [27], which calculated the mean annual power production of single-body WEC shapes. (The reader is referred to that study for more detail on the basis of our approach.) In the present study, 98 wave frequencies between $0.18 - 2.12 \text{rads}^{-1}$ are used to generate the response time series, with an integration step of 1s deemed sufficient for computing the average annual power capture. A modified Pierson-Moskowitz spectrum (p.24, [34]) is used to specify the frequency components present in each sea state. A motion cap is used to truncate the time series, based on practical considerations of the internal free surface for each design candidate.

5.3. Inner optimisation loop

It is assumed that only damping, and not stiffness, provision is feasible by each pneumatic PTO, and only the three diagonal damping matrix elements are considered. Similar to the approach used by McCabe [27], the damping coefficients are optimised for power extraction at the energy period of each sea state, giving 14 sets (14 energy periods cover all 173 considered sea states) of 3 coefficients, which are obtained using a gradient-based numerical solver.

5.4. Outer optimisation loop

A single-objective GA developed at the University of Sheffield [35], with extra adaptations to handle the constraints, forms the basic structure of the outer optimisation loop. A trial-and-error approach is taken to impose the physical constraints as hard boundaries on the search space, by repeating stages of the 'reproduction' process accordingly.

Figure 4 gives an overview of the full optimisation process.

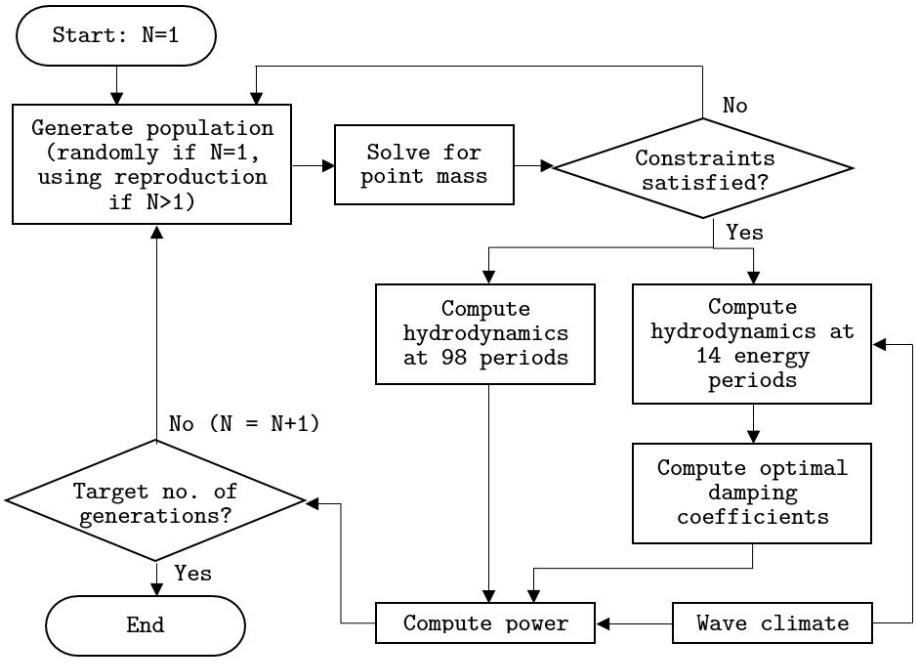

Figure 4: Outline of the structure of the full optimisation process. N is the generation number.

5.5. Variable bounds

The bounds on the optimisation variables (Table 1) are chosen to encompass a wide range of possible designs, whilst only allowing values that can lead to physically feasible devices. The tube wall thickness is set to 0.075m. Whilst

this value may be slightly too low for structural soundness of designs with L values near to the upper bound, the tube wall density could be adjusted to compensate. It must also be borne in mind that the simplified device design used in this study serves to represent the key characteristics, and adaptations to this would undoubtedly be required for a physical realisation.

Variable	Lower Bound	Upper Bound	Units
L	50	150	m
θ	20	60	$^\circ$
W	3.5	25	m
D	3.5	30	m
L_f	13	90	m
W_f	1.75	35	m
ρ_b	1000	6500	kgm^{-3}
ρ_f	50	900	kgm^{-3}

Table 1: Variable ranges used for GA runs.

6. Model accuracy and testing philosophy

Whilst the numerical method can enable an efficient assessment of many design candidates, there are other associated problems which must be mitigated by the optimisation algorithm in order to obtain sufficiently accurate outputs. These are manifested in two ways.

Firstly, the numerical solvers employed by WAMIT may not be able to adequately solve the system of equations. The complex geometry of the WaveTrain device and the accompanying interaction between the closely spaced modules make this phenomenon more likely than with simpler WEC designs. Whilst WAMIT's direct solver is the most robust option offered [10], numerical errors can still cause erroneous results. This was only found to occur for very specific combinations of the optimisation variables, but the genetic algorithm proved to be particularly adept at locating and exploiting these types of designs if they resulted in large overestimates of the power extraction. In order to effectively detect the occurrence of this type of error, a block-iterative solver is instead used, so that the numerical errors manifest as a failure of the solver to converge. Experience dictates that three blocks is most appropriate for this application, as this version of the solver retains levels of robustness very close to those of the direct solver, so should not result in the exclusion (from consideration by the genetic algorithm) of a significant number of designs.

If the maximum number of iterations (of 35) is reached for more than 10 of the 98 frequencies, then the power is set to zero for that individual. Below this limit, the power is set to zero at just the unconverged frequencies. In order to save on computational expenses and to ensure fewer 'zero-power' individuals in each GA generation, a preliminary check for solver convergence is also carried out for each individual, at six test wave periods (3, 4.5, 6, 9, 12 and 30s). If the maximum number of iterations is reached for more than one of these frequencies,

the individual is removed and replaced by another, before computing the full objective function.

The second way in which numerical problems can arise is through a lack of accuracy resulting from insufficient patch subdivisions (or 'panels') and/or orders of the B-splines. In applications focussing on a single WEC design, this is often handled by performing tests of the convergence of the hydrodynamic outputs with increasing numbers of panels (e.g. [36]). In an optimisation study where thousands of designs may be analysed, it is inefficient and impractical to adopt that approach. The rest of this section details the tools used to mitigate this difficulty, taking into account the objectives of the GA.

6.1. Maximising the utility of the GA

The purpose of this GA is to explore the features that lead to more optimal configurations of the WaveTrain device. Since only the best-performing designs are of interest, it is not essential that all devices tested have sufficiently accurate hydrodynamic results, just that those with inaccuracies do not skew the search enough to prevent the discovery of the optimal designs. If multiple GA runs are to be used to infer trends, then it is also not necessary that each GA run converges on a specific design, just that enough GA runs get close enough to the best designs (of which there may be many) to elucidate the true trends. The aim of such an optimisation scheme is to strike a compromise between computational demands and the thoroughness of the search, whilst maintaining both enough accuracy of the hydrodynamic outputs used to compute the objective functions, and enough convergence of each GA run. Thus, any tools that aim to improve the model accuracy of the designs encountered through the GA searches should be computationally efficient, and should not exclude so much of the search space that too little of it remains for a thorough investigation.

6.2. Tools for achieving maximal GA utility

Inaccuracies caused by excessively thin patches are mitigated by rectification of the geometry (Fig. 5).

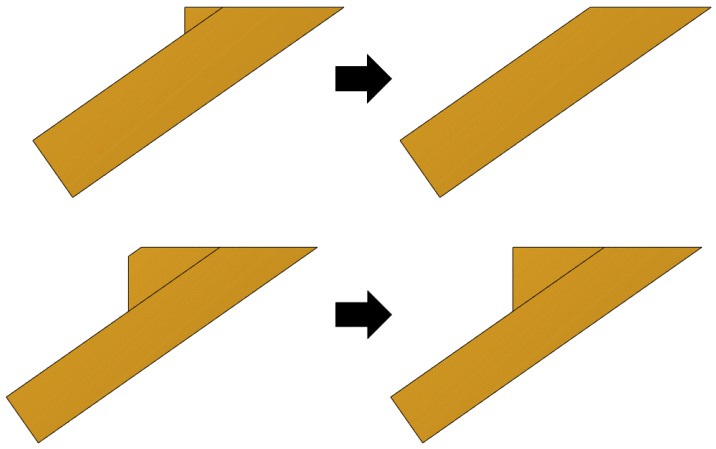

Figure 5: The geometry modifications applied to meshes that initially comprise a float patch deemed too thin to enable an accurate hydrodynamic analysis. Left: original meshes selected by the algorithm. Right: modified meshes.

Spurious peaks can also sometimes occur in the Response Amplitude Operator (RAO) magnitudes at high wave frequencies, due to a small wavelength to panel size ratio. In order to avoid the extra computational resources required by rerunning WAMIT with a finer discretisation at those frequencies, the peaks can simply be removed. As they occur at high frequencies, they are not likely to significantly affect the power generation of enough designs to skew the overall optimisation results (see again section 6.1). If the RAO magnitude of any of the three water column lids takes a value greater than unity for a wave frequency above 1.24rads^{-1}, this RAO value is set to zero. These thresholds used to detect the spurious peaks were determined empirically from the consideration of a range of possible optimisation designs.

Whereas the previous two tools modify an existing model to remove sources of inaccuracy, a direct check is also required as a final safeguard against the proliferation of inaccurate models. Theoretically, the added mass and radiation damping matrices are symmetric, but this does not hold if an insufficient number of panels (or an inappropriate spline order - see Appendix E) is used. Hence, by using just a single discretisation (the number of panels and the spline order), a measure of the amount of symmetry in these matrices can act as a proxy for the model accuracy. In this study, several of the off-diagonal added mass coefficients are considered, using an empirical threshold to exclude hydrodynamic models with insufficient accuracy. This process is applied firstly at the same six test periods (see the first part of Section 6) but also then over all 98 periods.

Bearing in mind the discussion in Section 6.1, there should still be areas of the search space in which model accuracy is less than perfect. These can be addressed with more thorough convergence studies on a subset of the best

performing designs (see Section 7).

7. Results and Discussion

The series of GA runs performed in this section is motivated by the nature of the search space and its impact on the performance of the GA. The WaveTrain concept is subject to physical constraints (Eqs. A.1 - A.4), overlaid with constraints due to the difficulties in finding sufficiently accurate numerical solutions to the hydrodynamic equations (i.e. the 'computational constraints' discussed in Section 6). Whilst the eight-dimensional search space cannot easily be visualised, some insight can be derived from the distributions of possible designs with respect to each of the optimisation variables. Figures 6 and 7 show the distributions of 7762 randomly-generated designs that satisfy the physical constraints, of which only 2000 are feasible by also satisfying the computational constraints. (Each variable range from Table 1 has been split into ten equally-sized sub-ranges.)

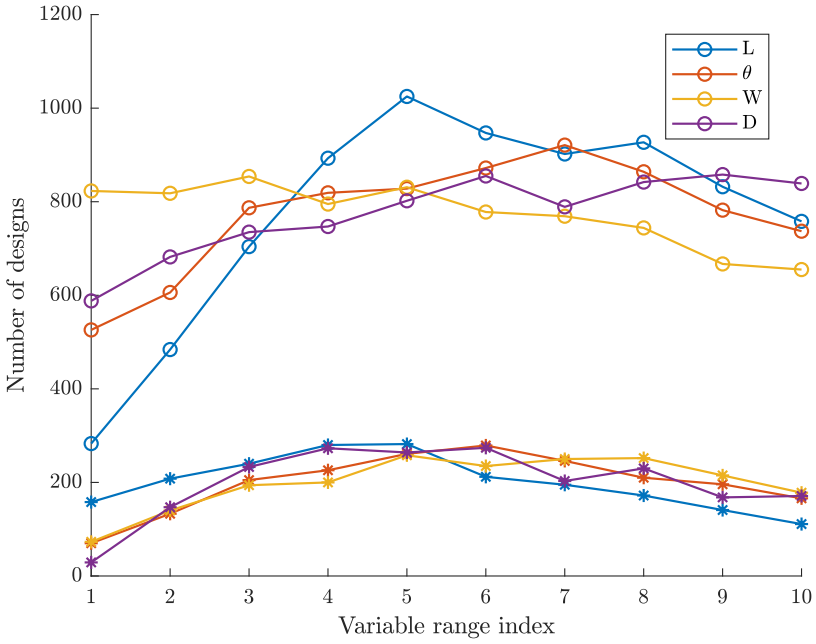

Figure 6: The distributions of WaveTrain designs within the allowed range of each optimisation variable, that satisfy both the physical and computational constraints (stars), and that satisfy only the physical constraints (circles).

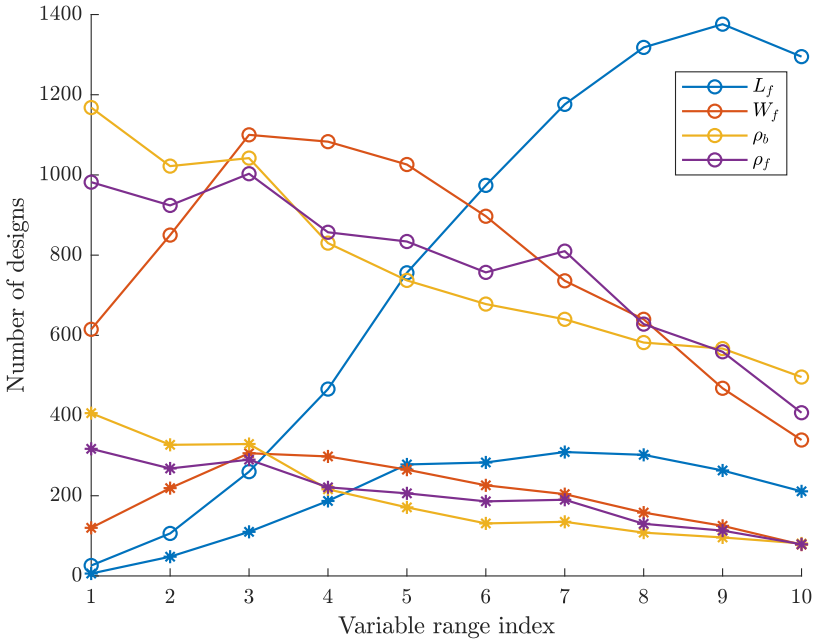

Figure 7: The distributions of WaveTrain designs within the allowed range of each optimisation variable, that satisfy both the physical and computational constraints (stars), and that satisfy only the physical constraints (circles).

Although the computational constraints further diminish the number of possible designs included in the optimisation study, the relatively unchanged shapes of the distributions can be used to make two pertinent observations: firstly, that the optimisation results should still reflect the underlying physics (and not be significantly skewed by the computational constraints); and secondly, the even spread of discontinuities across the feasible search space reinforces the need for a metaheuristic optimisation algorithm.

Another key consequence of this data is that designs of lower inclination angle, θ, are not as readily discovered and assessed as designs of greater θ (see Fig. 6). It is also unclear whether there will be just one optimal design. Especially given the discontinuous nature of the search space, the GA may well be predisposed to find multiple candidates for optimal performance. For these reasons, the GA is run multiple times within specific angle ranges. Each GA run uses 31 generations (including the initial population) of 16 individuals (twice the number of variables). 24 GA runs were made, three for each five degree range between 20 and 60°. To confirm the accuracy of the final results, the hydrodynamic model for each of the final generation individuals (most of which are near-optimal solutions) is compared for two discretisations: quadratic splines with a panel size of 20% of L, and cubic splines with a panel size of 10% of L. (See Appendix E for more detail on mesh discretisations and testing for

accuracy using the higher-order method, in the context of the WaveTrain as an application.) If the power differs by less than 5% between these two cases, the model is deemed to be suitably converged. Whilst power was used as the objective function, the computational constraints can sometimes restrict the GA's ability to increase the frontal width, D, of a given design, which tends to increase power capture. Hence, Capture Width Ratio (CWR) can be better placed to elucidate the pertinent design trends.

Before exploring the design trends that follow from analysis of the overall results, it is useful to examine the behaviour of the optimisation process. Figure 8 shows the evolution of the eight design variables through the 31 generations, for one of the three GA runs with $30° < \theta < 35°$. In the first generation, the variables are typically quite evenly distributed between their lower and upper bounds, and as the search proceeds, the distributions narrow as the algorithm converges towards a smaller number of regions of the search space. (Note, the few zero-power individuals shown reflect a failure of the computational constraints after making the full WAMIT run - see section 6.) In this GA run, the best designs (see the purple data points of Fig. 8) have L and D values virtually at their upper bounds, reflecting the tendency of increasing D and L to increase power extraction. The other six variables have, perhaps more interestingly, converged on intermediate values.

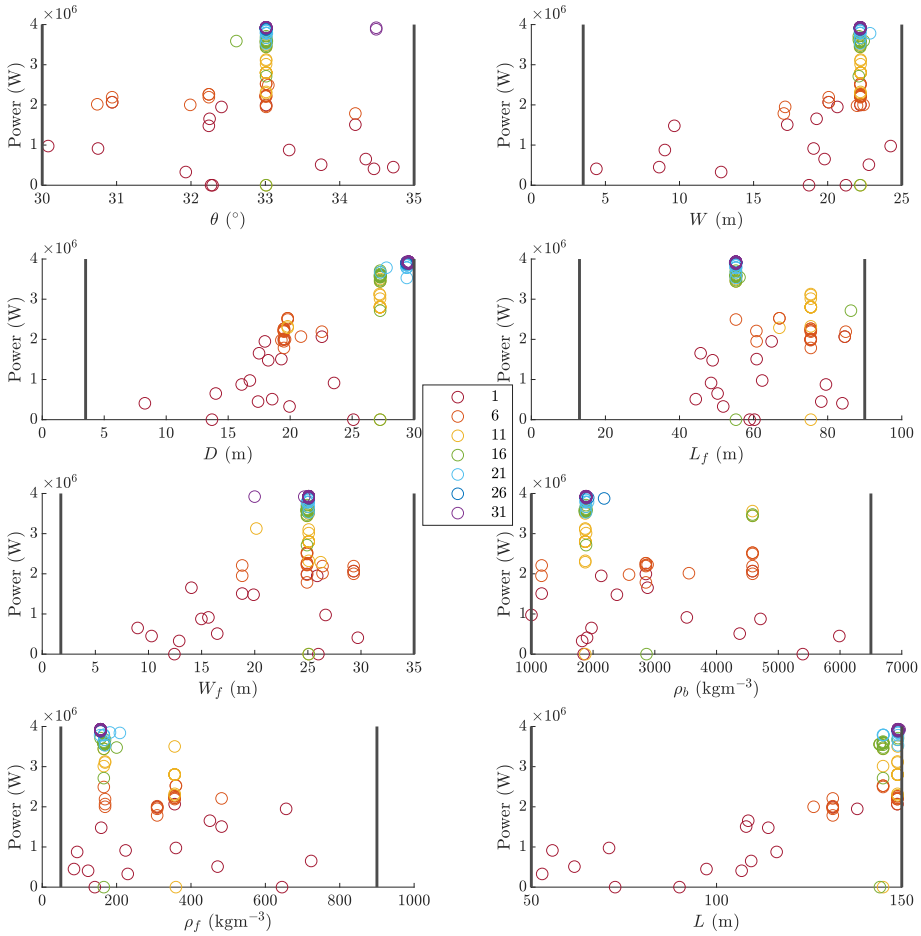

Figure 8: Evolution of the eight optimisation variables with the objective function through the 31 generations, for one of the 24 GA runs. Legend (at centre) defines the generation number. Vertical lines define the variable bounds.

Figure 9 shows the convergence of the objective function for the same particular GA run. In this case, the algorithm convergence is relatively smooth beyond around generation 10, as it is not visibly affected by the discontinuities. In parts of the search space where the infeasible regions are larger, this would not be the case, and the convergence may be expected to proceed more often through a series of more visibly discrete jumps.

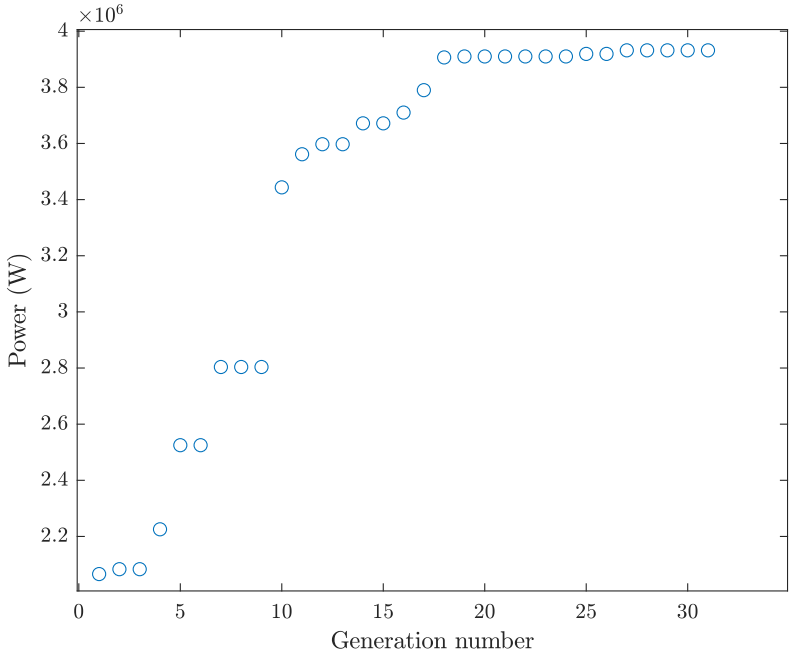

Figure 9: Convergence of the objective function towards at least a near-optimal design, for one of the 24 GA runs.

By now considering the total of 11904 individuals assessed by the GA, several design trends become apparent. Firstly, it appears important that the mass of entrained water within each module is sufficiently large relative to the module mass. In this context, the ratio of these two masses is a necessary but not sufficient condition for high power extraction (Fig. 10). In order to maintain a broad power absorption bandwidth, the resonant response of the entrained water columns and the modules must be sufficiently spaced in wave period. There is an upper limit on module mass (relative to the module size) due to the physical constraints (in particular, the device must not sink), whereas the mass of entrained water can be increased more freely. This provides an explanation as to why the mass ratio is a necessary condition, but it cannot be a sufficient condition as it does not completely embody the other design features presented hereafter. Designs with predicted CWRs above 2 are characterised by mass ratios ranging between 9 and 40 (Fig. 10). A region of perhaps more physically realisable designs has mass ratios around 5. Note that wave climates encompassing a wider range of wave periods would be expected to require higher values of the mass ratio, in order to achieve a broader profile of resonant response.

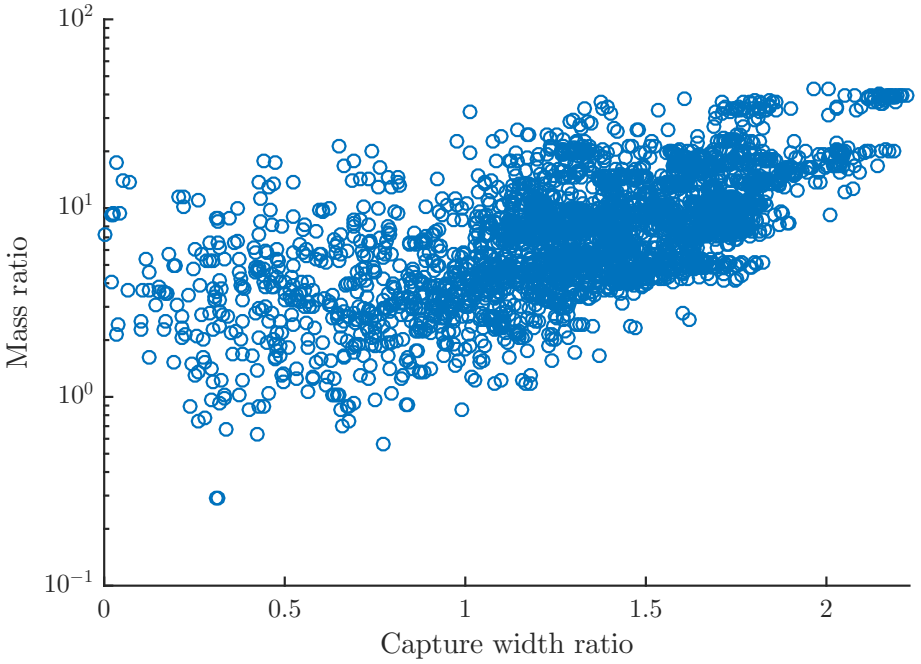

Figure 10: The mass ratio is defined as the mass of entrained water, divided by the mass of the module. Each data point represents one set of design parameters encountered by the GA.

Another parameter on which power capture (or CWR) depends strongly is the module inclination angle, θ. Fig. 11 shows that the highest performance can be attained with devices whose inclination angles are around 36°, but that relatively high performance can also be sustained towards higher and particularly lower values of θ. By highlighting the individuals (magenta data set in Fig. 11) for which convergence has been more rigorously tested, the trend is further justified, confirming that it is not simply an artefact. Again, this condition is necessary for optimal performance, but not sufficient, due to the dependency on other parameters such as the mass ratio.

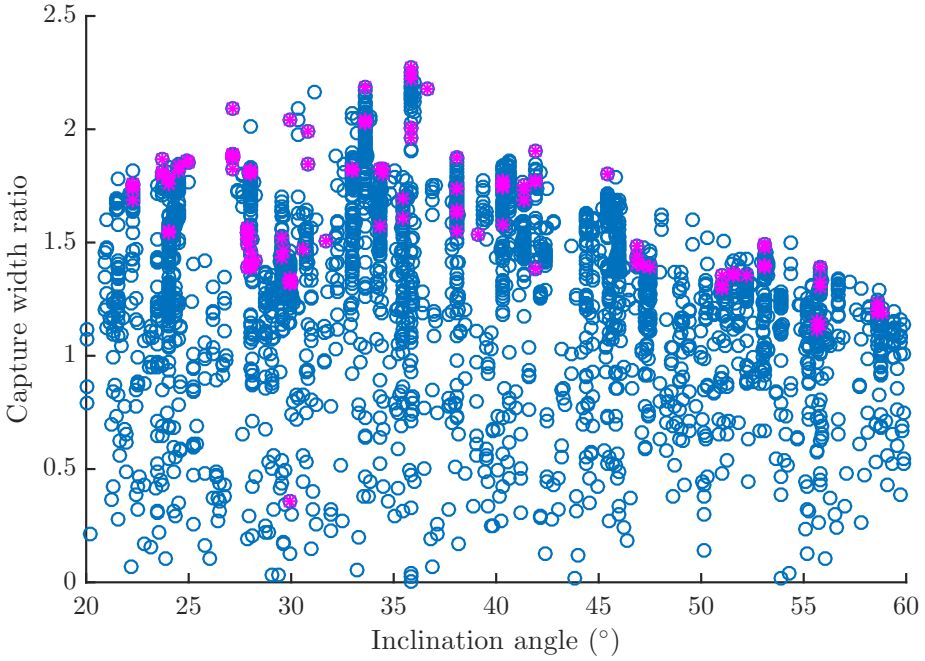

Figure 11: The dependence of capture width ratio on the module inclination angle. Blue circles represent all parameter sets encountered by the GA. Magenta stars represent only parameter sets from the final generations, whose hydrodynamic models are deemed suitably converged ($< 5\%$ difference in power between the two model discretisations). Also included are results from three extra GA runs, with $25° < \theta < 32°$, to help overcome the inherent bias against designs of lower θ.

Whereas the dimensions of the tube (L, D, W) approach their upper bounds, there is more variability of the other parameters amongst the best performing designs, yet with some ranges in which performance is better. Considering just devices with power extraction in excess of 3.5MW: L_f lies between 30 and 65m, ranging from 0.22 to 0.45 of the module length; W_f ranges from 10 to 28m; ρ_b ranges between the lower bound of 1000kgm^{-3}, up to values approaching 4000kgm^{-3}; ρ_f values remain towards the lower end of the allowed range, somewhere between 90 and 300kgm^{-3}. The spread of these variables increases further if lower power captures are considered. From this evidence, there are likely to be many near optimal designs, which could allow extra flexibility in construction without compromising on performance.

Despite the spread in many of the variables seen amongst the optimal devices, various combinations of them are required to fulfil other criteria necessary for high power capture. Firstly, the waterlines intersect the highest power extracting (> around 3.5MW) designs below the top of the Vertical Float Face (VFF) (Fig. 12). The waterlines intersect the very highest power designs halfway down the VFF. Again, this is not a sufficient condition, because variation of the other

parameters can reduce power extraction but retain the waterline position.

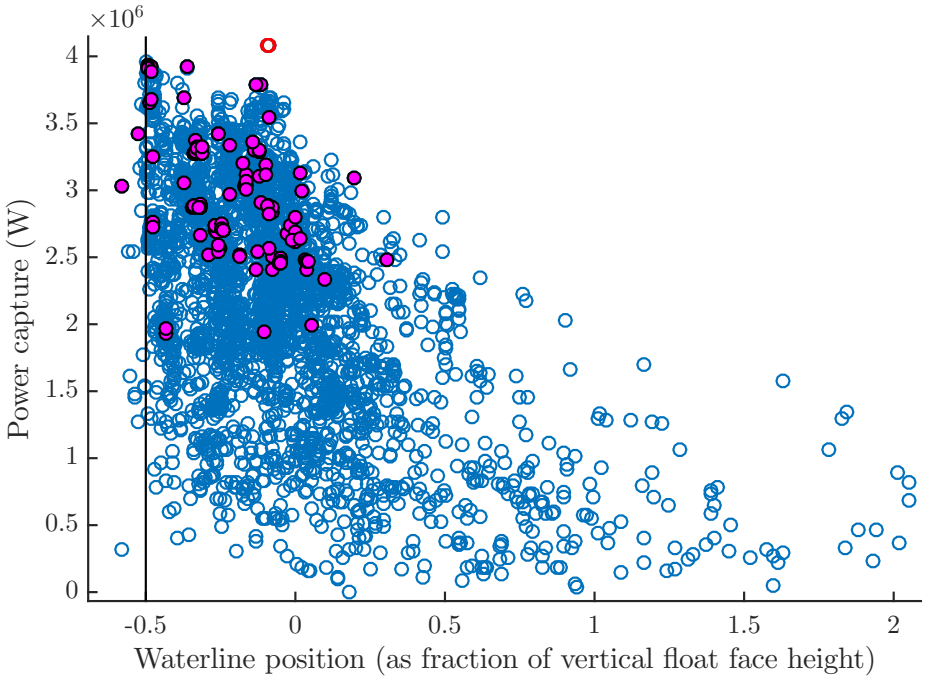

Figure 12: The relationship between the waterline position and the power capture. Blue circles represent all parameter sets encountered by the GA. Magenta circles represent parameter sets from the final generation, whose hydrodynamic models are deemed suitably converged. Red circles (very closely spaced) denote two final generation devices for which the hydrodynamic model accuracy is too low to be considered. A waterline position of zero corresponds to the top of the vertical float face, and a positive or negative value denotes the waterline position above or below this point, as a fraction of the total height of the vertical float face.

A similar criterion exists for the float width (W_f) employed in the group of high power extracting designs (again, $>$ around 3.5MW), where W_f is not less than half the maximum allowed value (Fig. 13). In fact, the very highest power extracting designs have W_f much closer to the maximum value (defined by the second relation of Eq. A.4), which would correspond to a triangular float shape. This bears great similarity to the trends observed for the waterline position, and is no coincidence, as shown by the relation between the two (Fig. 14).

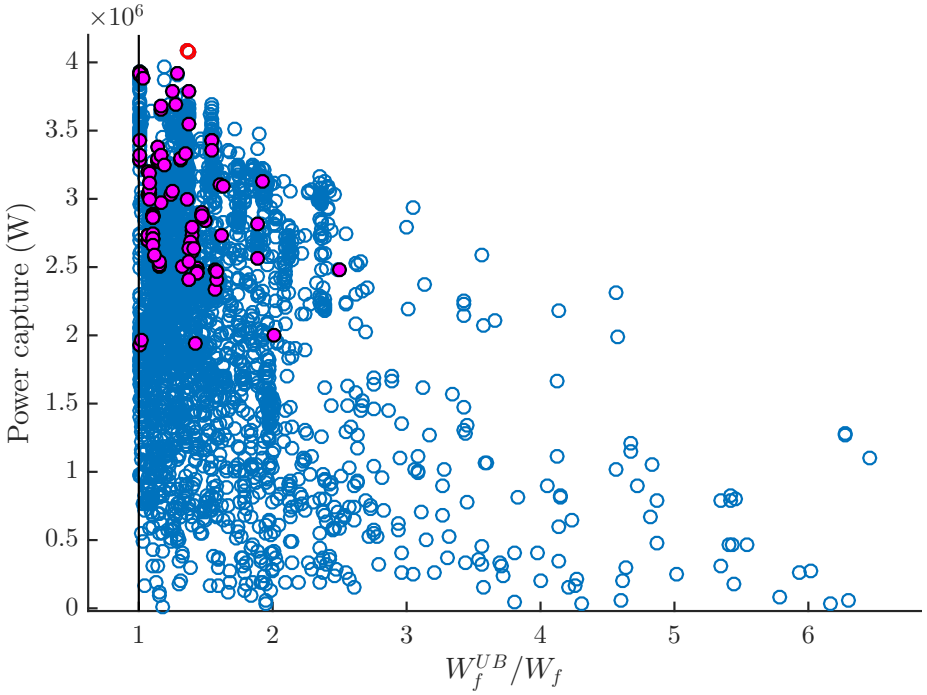

Figure 13: The relationship between the float width relative to the upper bound, and the power capture. Blue circles represent all parameter sets encountered by the GA. Magenta circles represent parameter sets from the final generation, whose hydrodynamic models are deemed suitably converged. Red circles (very closely spaced) denote two final generation devices for which the hydrodynamic model accuracy is too low to be considered.

Enforced by the physical constraints, all data points lie within a band that expands in thickness as it approaches thinner floats and higher relative waterline positions, but becomes sparser. The density of encountered parameter sets towards thicker floats and lower relative waterline positions reflects the convergence of the GA runs towards the higher performing individuals. It makes physical sense that for floats at the triangular limit, waterlines cannot lie above the VFF, since this would correspond to the device being fully submerged. Whilst there are no limits imposed through this linear model on how close to full submergence the device can be, there are signs that being close to this region is actually detrimental to the performance. In other words, not having enough mass above the water level, in general results in lower power capture, even when neglecting the changes in waterline that would occur in the physical system. This is reflected in the set of suitably converged ($< 5\%$ difference in power between the two test discretisations) individuals from the final generations of the GA runs (Fig. 14). These individuals are some of the highest power extractors, and always allow a significant amount of the body to lie above the water surface. Though not the strongest correlation, designs with thicker floats tend to benefit from a lower relative waterline position, which retains a

significant amount of the device above water. Conversely, amongst these higher power designs, a higher relative waterline position is only beneficial if the float is thinner.

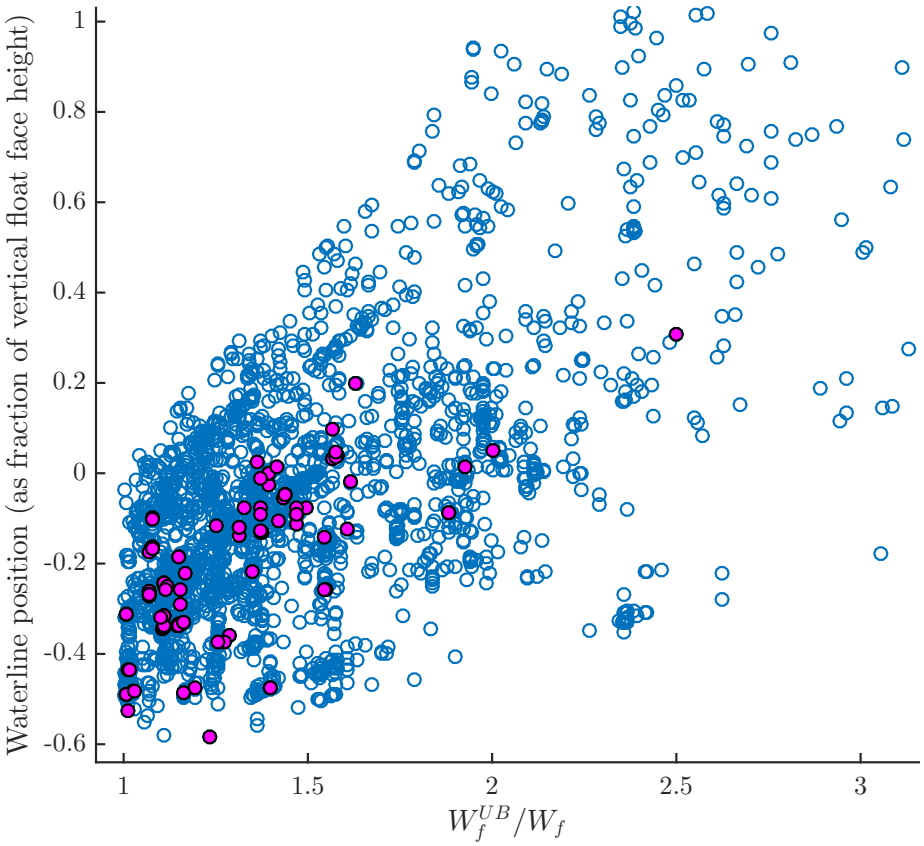

Figure 14: The relationship between the waterline position and the float width relative to the upper bound. Blue circles represent all parameter sets encountered by the GA. Magenta circles represent parameter sets from the final generation, whose hydrodynamic models are deemed suitably converged. A waterline position of zero corresponds to the top of the vertical float face, and a positive or negative value denotes the waterline position above or below this point, as a fraction of the total height of the vertical float face.

8. Conclusions

In order to retain the beneficial features of sloped motion in a deep water environment, a novel WEC concept has been introduced. This concept (the 'Wave-Train') exploits a mechanical interlinking of multiple sloped modules, using rotational joints in order to restrict the counterproductive pitch motions through the provision of restorative forces that can be exchanged between neighbouring modules. As a result of the complex set of design constraints, prior testing

had not been afforded the opportunity for a thorough optimisation of the mass distribution and geometry, motivating the need for an efficient hydrodynamic model. Given the scarcity in the literature of details regarding the implementation of generalised modes of motion for jointed bodies, a didactic treatment has been given alongside the development of an efficient hydrodynamic model. Due to the complex body geometry, the set of physical constraints, and the limited numerical solver capabilities, the use of the numerical model in computing the objective function necessitated the development of bespoke optimisation routines based upon a genetic algorithm (GA). An inner optimisation loop was used to optimise the power take-off damping coefficients of each design. How best to maximise the utility of the optimisation routines was discussed, primarily with regards to the challenges in achieving accurate hydrodynamic model results across a significant enough fraction of the search space. Six geometric variables and two variables relating to the mass distribution were used to optimise the annual mean power extraction in a wave climate based on data from a site on the West Shetland Shelf in the North East Atlantic Ocean. 24 GA runs, each with 31 generations of 16 individuals, were carried out for specific angle ranges, to provide the majority of the study results. Extra tests of accuracy were performed for final generation individuals, in order to verify the resulting trends.

Whilst it was discovered that there does not exist any single design that significantly outperforms all others, five key design criteria have been discovered. All appear as necessary but not sufficient conditions.

The ratio of the mass of the internal water column to the mass of the surrounding module must be sufficiently large, in order to space the resonant response of those two elements appropriately in wave frequency. The exact value of the ratio required is somewhat dependent on the geometric and mass parameters chosen, but a value of at least five is recommended. Should stronger low density materials become available in the near future, even greater mass ratios would be better advised. It must also be borne in mind that a wave climate experiencing a narrower range of frequency components would likely require lower mass ratios than those recommended here.

The optimal inclination angle of each WaveTrain module lies around 36°, but significant powers and CWRs can still be obtained between 27 and 37°.

The final three criteria are more evidently dependent on one another. The thickest floats (W_f closest to the upper limit enforced by L_f) tend to be required to produce the best performance, whilst the waterline in those designs must be low enough that it leaves a sufficient amount of bulk above the water surface. In these designs, the best waterline position is around halfway down the vertical float face (VFF). In summary, the optimal configurations involve an almost maximal vertical float face height (provided by maximal W_f), with a waterline intersecting very close to halfway down the VFF. However, provided that a sufficient amount of bulk is retained above the water surface, slightly less-than-optimal designs exist with float widths as narrow as half the maximum allowed value, and with waterlines intersecting positions all the way up to the top of the VFF. Significant power reductions can be expected with floats any narrower

than this, and with waterlines intersecting any higher than the VFF.

These five criteria (mass ratio, θ, waterline height, relative float width, and the amount of 'bulk' above water) vastly narrow the remaining area of design space. However, there remains flexibility in the choice of the other parameters, providing some scope for practical considerations relating to the available materials and construction techniques. Whilst for the highest power-extracting designs in this study, the upper bounds of W, D, and L were pushed up against, the remaining four parameters were not so tightly constrained: L_f ranged between 30 and 65m (between 0.22 and 0.45 of the module length, L), W_f ranged from 10 to 28m, ρ_b ranged from the lower bound of 1000kgm^{-3} up to values approaching 4000kgm^{-3}, and ρ_f ranged somewhere between 90 and 300kgm^{-3}.

Acknowledgements

This work was supported by a studentship provided by the EPSRC through the Wind and Marine Energy Systems Centre for Doctoral Training [award reference 1809924].

The authors would also like to thank Dr. Nicholas Wells and Dr. Jos van 't Hoff for introducing them to the WaveTrain device concept and for motivating this optimisation study.

Appendix A. Physical constraints

There are a number of constraints that need to hold to ensure physical feasibility. Firstly, the centre of buoyancy of a given module must lie on the same vertical line as the centre of gravity, for the desired inclination angle to be achieved at equilibrium (Eq. A.1).

$$x_B = x_G \tag{A.1}$$

It is also imperative that the device as a whole does not capsize when displaced, and instead returns to its equilibrium position - i.e. static stability is observed. Additionally, each individual module must be statically stable, to maintain the intended device configuration. The stability of the entire chain of modules is implied by each individual module being statically stable, and just considering in-plane motions, each module must be statically stable in pitch. This is equivalent to requiring positive metacentric heights (Eq. A.2).

$$(S_{11}/\forall) + z_B - z_G > 0 \tag{A.2}$$

S_{11} denotes a waterplane moment associated with pitch rotation (see [37], p.292), $\forall$ denotes the displaced water volume.

In order for the vertical float face to correctly influence the device dynamics, the equilibrium water level should be no lower than the bottom of this vertical surface. The fact that the device should not be fully submerged enforces an upper constraint on the waterline. Since the height at which the module

rests in equilibrium is dependent on its mass distribution, these waterline limits correspond to upper and lower bounds on the module mass (Eq. A.3).

$$M_{LB} \leq M \leq M_{UB} \tag{A.3}$$

Two further physical constraints are imposed by the float configuration (Eq. A.4). Firstly, the float must be shorter than the tubes. Secondly, due to the lower and upper side surfaces of the float being vertical and horizontal, respectively, the float width must be less than than its value in the extreme case where the top of the trapezium has zero length (i.e. where the float is triangular in shape).

$$L_f < L \text{ and } W_f < L_f sin(\theta) cos(\theta) \tag{A.4}$$

This forms a set of six constraints, which any feasible design must satisfy.

Appendix B. Hinges - an applied didactic treatment

Whilst the choice is not unique, the type of shape function adopted here to define the hinge modes of motion follows naturally from consideration of the motions of a rigid body. (This also relevant to the construction of C_{ij} later in this section.) Assuming both small body motions and retaining only first order terms, Eq. B.1 relates a body coordinate, $\mathbf{x_{rb}} = [x, y, z]^T$ expressed in a fixed coordinate system to the same body coordinate $\mathbf{x'} = [x', y', z']^T$ expressed in a displaced coordinate system ([37], p.290).

$$\mathbf{x_{rb}} = \begin{bmatrix} 1 & -\xi_6 & \xi_5 \\ \xi_6 & 1 & -\xi_4 \\ -\xi_5 & \xi_4 & 1 \end{bmatrix} \mathbf{x'} + \begin{bmatrix} \xi_1 \\ \xi_2 \\ \xi_3 \end{bmatrix} \tag{B.1}$$

Now suppose there is a hinge at a location, $[a, b, c]^T$, about which the body is free to rotate in the x-z plane, and assume that some of the body is connected to one hinge arm ('left part'), and some to the other ('right part'). To operate as a hinge, the angle between the two parts of the body must change from its equilibrium angle - it may be that the 'left part' moves clockwise about the hinge, whilst the 'right part' rotates in an anticlockwise direction (as viewed from the same side of the body). Now consider a point on the 'left part' where clockwise rotation is positive, as it is for pitch rotation of the entire body. In order to express that point's displaced coordinates in the fixed coordinate system, accounting for this extra type of rotation, we must first shift to the hinge location, then apply the rotation about the y-axis, before shifting back to the origin of the fixed coordinate system (Eqs. B.2, B.3). Again, the rotation matrix is defined for small motions and only linear terms are retained.

$$\mathbf{x} = \begin{bmatrix} 1 & 0 & \xi_7 \\ 0 & 1 & 0 \\ -\xi_7 & 0 & 1 \end{bmatrix} \cdot \left(\mathbf{x_{rb}} + \begin{bmatrix} -a \\ -b \\ -c \end{bmatrix} \right) + \begin{bmatrix} a \\ b \\ c \end{bmatrix} \tag{B.2}$$

$$\mathbf{x} = \begin{bmatrix} x' + \xi_1 - \xi_6 y' + \xi_5 z' + \xi_7 (z' - c) \\ y' + \xi_2 - \xi_4 z' + \xi_6 x' \\ z' + \xi_3 + \xi_4 y' - \xi_5 x' - \xi_7 (x' - a) \end{bmatrix} \tag{B.3}$$

An appropriate shape function for the hinge is given by the components of $\mathbf{x}$ proportional to ξ_7. Defining the rotation oppositely would just result in opposite signs of the ξ_7 terms, and additional hinges would simply yield additional analogous terms due to the linearity of the transformation. Here, a symmetric form is rather arbitrarily opted for (this is not a unique choice), where the rotation of the 'right part' is defined oppositely to that of the 'left part' (Eq. B.4). Note that $x < a$ and $x > a$ are used as shorthand to denote the 'left part' and 'right part' of the body, respectively. Often these are equivalent, as in the case of the WaveTrain, but this is not true in general, as the mass connected to one hinge arm may surround the hinge.

$$\begin{aligned} \mathbf{S}_7(\mathbf{x}) &= \begin{bmatrix} z - c \\ 0 \\ -(x - a) \end{bmatrix} \text{ for } x < a \\ &= \begin{bmatrix} -(z - c) \\ 0 \\ x - a \end{bmatrix} \text{ for } x > a \end{aligned} \tag{B.4}$$

In this study, the assembly of three WaveTrain modules is treated as a single rigid body, to which the standard surge, heave and pitch modes are assigned. For simplicity, the origin of this coordinate system is set to coincide with the centre of gravity. In WAMIT, generalised modes are defined relative to the rigid body modes. Thus, any external torques applied at the hinges (e.g. by a power take-off system) will naturally provide the necessary reaction forces acting on the rest of the body. This simplifies the definition of the power take-off forces for a freely-floating wave energy converter.

Next, the mass and inertia couplings between each pair of modes are computed using Eq. B.5, where V_b is the volume of the body in its equilibrium position. Note that, in general, the shape functions may be non-zero only on a subset of the total body volume. In order to avoid further complicating the shape functions with this type of discontinuity, the integral limits can be altered instead. With this perspective, V_b is the intersection of the two total body volumes associated with modes i and j. For couplings between hinge modes and other hinge modes or rigid body modes, this is the entire body volume.

$$M_{ij} = \iiint_{V_b} \rho_b(\mathbf{x})(\mathbf{S}_i \cdot \mathbf{S}_j) dV \tag{B.5}$$

For complex shapes (such as the WaveTrain concept), where the body density is a non-trivial function of the spatial coordinates, and where there are many generalised modes, computing this matrix can be difficult or time-consuming, from both computational and human standpoints.

Finally, the gravitational forces/moments acting on each mode, due to a motion of each other mode, are found by Eq. B.6. The integral is taken over the instantaneous volume, $V_b^{(t)}$, since the quantity itself is dependent on the distinction between the fixed and displaced coordinate systems. This means that the shape functions, $\mathbf{S}_i$, ordinarily (and for the purposes of WAMIT) defined in the fixed coordinate system, must be re-expressed in the displaced coordinate system if the integration is to be more conveniently performed over the equilibrium volume, V_b. This is done by substituting Eq. B.3 into Eq. B.6, for a given shape function. Combining this with Eq. B.7 allows determination of the coefficients, C_{ij}, that are first-order in the body motions. The zeroth-order forces are not considered as these are cancelled by the buoyancy forces for a body freely floating about its equilibrium position.

$$F_i = -g \iiint_{V_b^{(t)}} \rho_b(\mathbf{x})(\mathbf{S}_i \cdot \hat{\mathbf{k}}) dV \tag{B.6}$$

$$F_i = -\sum_{j=1}^{N} C_{ij}\xi_j \tag{B.7}$$

Returning to the earlier example involving the six rigid body modes and a single hinge, Eqs. B.8 - B.10 illustrate an example case for C_{57}, the gravitational restoring moment acting on the rigid body pitch mode, due to a unit motion of the symmetric hinge mode. In the displaced coordinate frame, $V_b^{(t)} = V_b$. The discontinuity of the shape function leads to two force terms, one due to the body either side of the hinge. In physical terms, the coupling force is zero if there are equal moments about either side of the hinge, which is as expected, since a pitching of the body requires an uneven distribution of moments about its centre of rotation.

$$\begin{aligned} F_5 &= -g \iiint_{V_b^{(t)}} -x\rho dV \\ &= -g \iiint_{V_b} -(x' + \xi_1 - \xi_6 y' + \xi_5 z')\rho dV \\ &\quad - g \iiint_{V_{b,l}} -\xi_7(z' - c)\rho dV \\ &\quad - g \iiint_{V_{b,r}} \xi_7(z' - c)\rho dV \end{aligned} \tag{B.8}$$

$$F_{57} = (m_l g z_{g,l} - m_r g z_{g,r})\xi_7 \tag{B.9}$$

$$c_{57} = m_r g z_{g,r} - m_l g z_{g,l} \tag{B.10}$$

In the above equations, m_r denotes the mass to the right of the hinge (in this example, where $x > a$), and $z_{g,r}$ denotes the z-coordinate of the centre of gravity of the mass to the right hand side of the hinge, expressed relative to the hinge location. V_b is the equilibrium volume, and $V_{b,l}$ denotes the component of V_b residing to the left of the hinge (where $x < a$).

Appendix C. Ensuring physically feasible designs

The centre of gravity is the combined centre of mass of the float, tube and point mass. Quantifying the dependence of the centre of buoyancy on the point mass also requires knowledge of the volume distribution of the module, which is discontinuous as a function of height. Also bearing in mind the restrictions on waterline position, it is therefore useful to split the module cross-section into two zones, in each of which this volume function is continuous. This will yield a separate version of equation A.1 for each zone. Zone 1 spans the waterline locations that intersect the vertical float face. Zone 2 spans the regions between the top of zone 1 and the maximum waterline height (the top of the body).

In determining how x_B depends on the mass of the point mass, m_{pm}, it is useful to notice that x_B depends on the waterline position, h (defined from the lowest part of the module), which in turn depends on m_{pm}. Equating the displaced water mass with the total module mass (Archimedes' principle), h can be determined as a function of m_{pm} for each zone, i (Eqs. C.2, C.4). By substituting the upper and lower limits of h into these relations, the bounds for each zone can be reexpressed in terms of m_{pm} (Eq. C.1).

$$m^i_{pm_{LB}} \leq m_{pm} \leq m^i_{pm_{UB}} \tag{C.1}$$

This then allows equation A.1 to be expressed (for each zone) as a function of a single variable, and solved for m_{pm}.

For zone 1, this gives a fifth order polynomial equation in h, and a second order equation relating m_{pm} to h (Eqs. C.2, C.3). Equation C.3 can then be solved numerically, and its solution substituted into Eq. C.2 to obtain the m_{pm} that solves the constraint expressed by Eq. A.1, should one exist. Only solutions that also fall within one of the pairs of zone boundaries (Eq. C.1) are taken to represent physical solutions. For many parameter sets there will exist no physical solutions in either zone.

$$m_{pm} = A_1 h^2 + A_2 h + A_3 \tag{C.2}$$

$$B_1 h^5 + B_2 h^4 + B_3 h^3 + B_4 h^2 + B_5 h + B_6 = 0 \tag{C.3}$$

The corresponding two equations for zone 2 are of lower order (Eqs. C.4, C.5), due to the differing module cross-section shapes in each region - zone 1 includes a triangular element, zone 2 does not. These can be solved in a similar manner to equations C.2 and C.3.

$$m_{pm} = C_1 h + C_2 \tag{C.4}$$

$$D_1 h^3 + D_2 h^2 + D_3 h + D_4 = 0 \tag{C.5}$$

The constant coefficients of these polynomial equations, A_i, B_i, C_i and D_i, are functions of the nine fundamental geometric and density parameters that are known for a given device (see Fig. 3).

Appendix D. West Shetland Shelf wave climate

The annual occurrence matrix for the West Shetland Shelf wave climate used in this study is given in Table D.2 [27], in terms of mean zero-crossing period, T_z, and significant wave height, H_{m0}. The site is around 40km west of the Shetland Islands.

T_z (s) $\rightarrow$ H_{m0} (m) $\downarrow$	4.5	5.5	6.5	7.5	8.5	9.5	10.5	11.5	12.5	13.5	14.5	15.5	16.5	17.5
0.25	0	2	2	0	0	1	0	0	0	0	0	0	0	0
0.75	36	89	147	128	95	44	18	10	1	4	4	1	0	0
1.25	51	229	228	306	339	215	82	42	12	6	6	1	0	0
1.75	2	115	184	208	302	269	177	92	24	14	4	2	1	1
2.25	0	21	165	184	202	231	205	115	67	26	18	8	1	1
2.75	0	1	63	153	158	142	193	142	84	47	21	11	1	1
3.25	0	0	5	105	147	103	125	136	92	58	30	10	5	1
3.75	0	0	1	31	113	100	89	92	79	48	33	12	3	1
4.25	0	0	0	5	51	86	77	69	53	42	33	14	6	3
4.75	0	0	0	0	20	62	65	51	43	39	31	17	6	2
5.25	0	0	0	0	2	22	59	47	36	28	23	13	2	4
5.75	0	0	0	0	0	5	38	45	23	16	25	10	2	0
6.25	0	0	0	0	0	1	14	39	17	15	21	5	1	1
6.75	0	0	0	0	0	0	4	24	21	13	11	4	2	0
7.25	0	0	0	0	0	0	1	14	17	11	6	2	2	0
7.75	0	0	0	0	0	0	0	8	16	11	4	2	1	0
8.25	0	0	0	0	0	0	0	4	14	10	3	2	1	1
12.00	0	0	0	0	0	0	0	2	19	26	26	11	2	2

Table D.2: West Shetland Shelf occurrence matrix ($\hat{O}$, hours).

Appendix E. Mesh discretisations using the higher-order method

In order to test for sufficient accuracy of the hydrodynamic solution for a particular device, the problem is typically solved for a range of mesh discretisations, to see if the solution converges as the discretisation is made finer (see e.g. [36]). Using the low-order method, where the velocity potential is assumed constant at discrete points on the body surface, this amounts to simply increasing the number of those discrete points (defined by the number of panels).

In the higher-order method (see Chapter 7 of [10]), the velocity potential is represented continuously using B-spline basis functions. Each surface patch can be subdivided into a number of panels, using a different basis function on each. The accuracy of the hydrodynamic solution is then dependent on both the number of panels and the order of the B-splines. It is most often the case that increasing the spline order from constant (equivalent to the low-order method) to linear results in a more accurate solution [10][38]. However, it is

not necessarily the case that all subsequent increases in the spline order will increase the accuracy [38].

It is advised that quadratic or cubic B-splines are generally appropriate to represent the velocity potential [10]. However, this warrants some investigation, given the novel use case of the WaveTrain. The Response Amplitude Operators (RAOs) shown in this section are for the central water column, and are undamped. Whilst the RAOs are unrealistic, this represents the case that is most sensitive to inaccuracy in the solution, and so can most clearly show any differences. The 'PANEL_SIZE' parameter of WAMIT has been used to easily change the number of panels across all surfaces (see [10]).

In our experience, it is certainly the case that quadratic B-splines can be sufficient for WaveTrain models. In many cases, it is also only necessary to increase the number of panels in order to test convergence (e.g. see Figure E.15, along with Table E.3), in a similar manner to a typical convergence test using the low-order method.

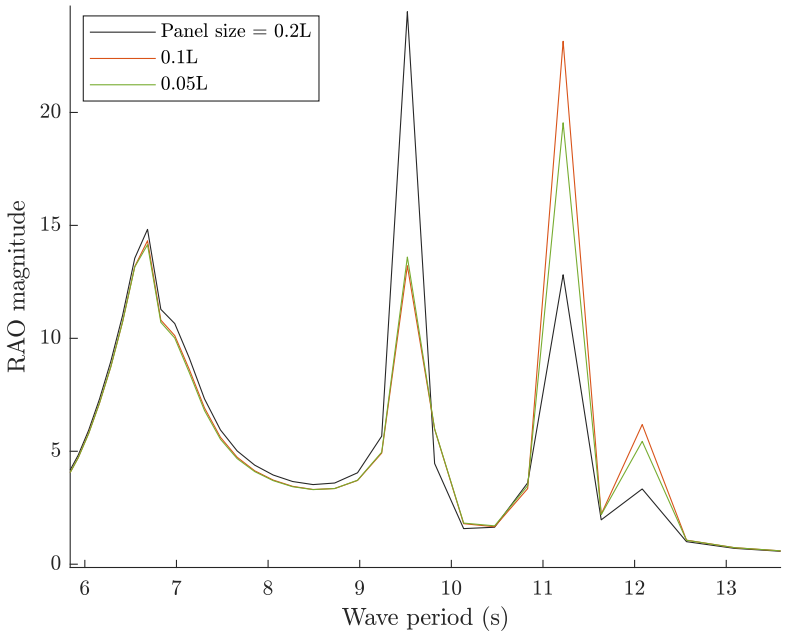

Figure E.15: Convergence of central water column RAO, for test device 1.

Parameter	Value
L	46.14
θ	39.36
W	5.18
D	9.48
L_f	22.12
W_f	4.27
ρ_b	339.34
ρ_f	74.26

Table E.3: Test device 1.

However, we have also discovered designs that highlight the need to additionally consider the spline order in such tests of accuracy. For example, Figure E.16 shows the RAOs for a different WaveTrain design (see Table E.4). Based on just the largest two panel sizes shown (0.1L and 0.2L), it appears that the larger panel size (with quadratic spline order) may be sufficient. However, further decreasing the panel size to 0.05L produces a vastly different RAO plot and brings this into question.

In this case, a cubic spline order is more appropriate - see the improved convergence of the RAOs in Figure E.17 as the panel size is decreased. The close match between the black plots of Figures E.16 and E.17 indicates that quadratic splines with a panel size of 0.2L is in fact sufficient for this particular design. However, one may be misled if the spline order were not also considered (along with the number of panels) in a convergence test. (For the WaveTrain, we also found that the numerical solvers of WAMIT were usually not able to obtain a solution with spline orders greater than 3.)

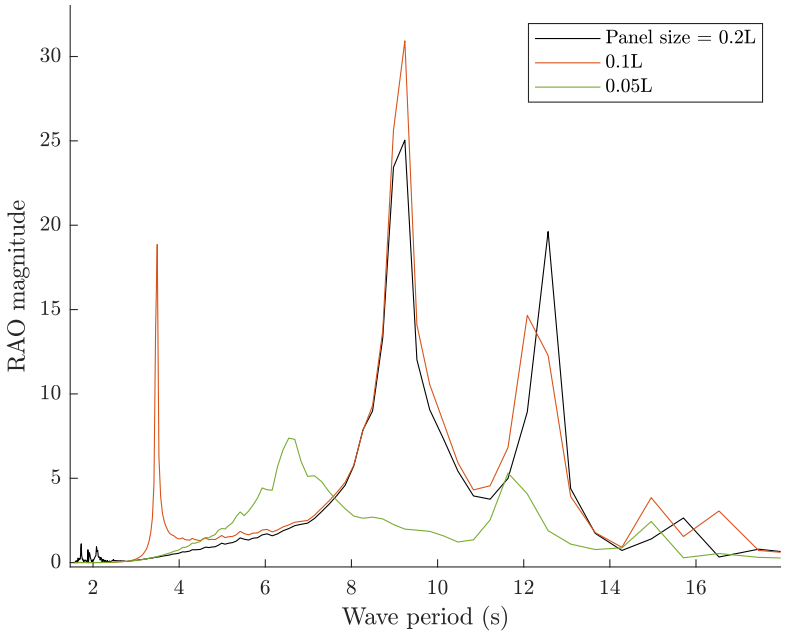

Figure E.16: Poor convergence of central water column RAO is due to inadequate order of B-spline.

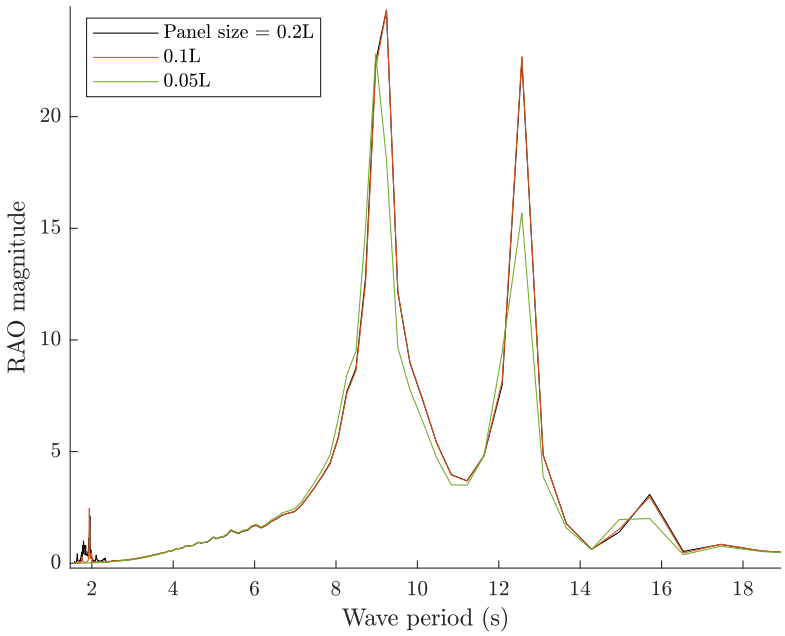

Figure E.17: Convergence of central water column RAO is much improved using cubic B-splines.

Parameter	Value
L	88.77
θ	43.42
W	16.59
D	14.46
L_f	30.42
W_f	3.38
ρ_b	647.31
ρ_f	134.75

Table E.4: Test device 2.

In our experience, a panel size of 0.2L with quadratic splines strikes a sufficient compromise between runtime and accuracy, which allows for a maximally large search space of feasible designs, given the available computational resources.

A reduction of the panel size to 0.1L and an increase in the spline order by one (to cubic splines) was found to be a reliable test for sufficient convergence of the optimisation results.

Figure E.15 also indicates the differing levels of accuracy of the solution at different wave periods - the difference between the three RAO plots is much smaller at lower wave periods. This suggests a frequency-dependent discretisation may be optimal. However, this has not been pursued in this study, partly because of the increase in runtime that would result from having to initialise separate WAMIT runs at each wave period.

References

[1] A. F. de O. Falcão, Wave energy utilization: A review of the technologies, Renewable and Sustainable Energy Reviews 14 (2010) 899–918. doi:10.1016/j.rser.2009.11.003.

[2] S. A. Noren, Apparatus for recovering the kinetic energy of sea waves, US Patent No. 4773221 (1982) .

[3] S. Salter, C.-P. Lin, The sloped IPS wave energy converter, 2nd European Wave Power Conference (1995) 337–344.

[4] C.-P. Lin, Experimental studies of the hydrodynamic characteristics of a sloped wave energy device, PhD thesis, University of Edinburgh (1999) .

[5] G. Payne, J. Taylor, T. Bruce, P. Parkin, Assessment of boundary-element method for modelling a free-floating sloped wave energy device. part 2: Experimental validation, Ocean Engineering 35 (2008) 342–357. doi:10.1016/j.oceaneng.2007.10.008.

[6] P. Parkin, G. Payne, J. Taylor, Numerical simulation and tank tests of the free-floating sloped IPS buoy, 5th European Wave Energy Conference (2003) .

[7] N. Wells, B. Elsaesser, Performance of the JOULES Wavetrain WEC, MARINET Infrastructure Access Report (2013, accessed on 04/06/20).
URL http://www.marinet2.eu/wp-content/uploads/2017/04/Wavetrain_HMRC_Infrastucture_Access_Report-1.pdf

[8] A. Cotten, J. van 't Hoff, D. Forehand, N. Wells, Numerical and physical modelling of a novel, sloped module, multibody wave energy converter, 3rd International Conference on Offshore Renewable Energy (2018) 48–57.

[9] WaveTrain sloped pneumatic WEC, Wave Energy Scotland Novel Wave Energy Converter Programme, Stage 1, http://www.waveenergyscotland.co.uk/programmes/details/novel-wave-energy-converter/wavetrain-sloped-pneumatic-wec/, accessed on 04/06/20.

[10] WAMIT User Manual (v7.2), WAMIT Inc., http://www.wamit.com/manual.htm, accessed on 04/06/20.

[11] J. N. Newman, Wave effects on deformable bodies, Applied Ocean Research 16 (1994) 47–59. doi:10.1016/0141-1187(94)90013-2.

[12] J. C. McNatt, V. Venugopal, D. Forehand, A novel method for deriving the diffraction transfer matrix and its application to multi-body interactions in water waves, Ocean Engineering 94 (2015) 173–185. doi:10.1016/j.oceaneng.2014.11.029.

[13] T. Mathai, Use of generalised modes in hydrodynamic analysis of multiple bodies, 10th International Offshore and Polar Engineering Conference (2000) .

[14] J. N. Newman, Wave effects on hinged bodies: Part 1 - body motions (1997, accessed on 04/06/20).
URL http://www.wamit.com/Publications/Hinged1.pdf

[15] C.-H. Lee, J. N. Newman, An assessment of hydroelasticity for very large hinged vessels, Journal of Fluids and Structures 14 (2000) 957–970. doi:10.1006/jfls.2000.0305.

[16] Y. Li, H. Peng, W. Qiu, B. Lundrigan, T. Gardiner, Hydrodynamic analysis and optimization of a hinged type wave energy converter, 35th International Conference on Ocean, Offshore and Arctic Engineering (2016) .

[17] S. Xu, J. M. Rodrigues, C. G. Soares, Hydrodynamic analysis and optimization of a wave activated device, Progress in Renewable Energies Offshore: Proceedings of the 2nd International Conference on Renewable Energies Offshore (2016) 285–292.

[18] X.-S. Yang, Optimization techniques and applications with examples, John Wiley & Sons Inc. (2018) doi:10.1002/9781119490616.

[19] X.-S. Yang, Introduction to algorithms for data mining and machine learning, chaper 3: Optimization algorithms, Academic Press (2019) 45–65doi:10.1016/B978-0-12-817216-2.00010-7.

[20] D. W. Zingg, M. Nemec, T. H. Pulliam, A comparative evaluation of genetic and gradient-based algorithms applied to aerodynamic optimization, European Journal of Computational Mechanics 17 (2012) 103–126. doi:10.3166/remn.17.103-126.

[21] K. C. Giannakoglou, D. I. Papadimitriou, Optimization and computational fluid dynamics, chapter 4: Adjoint methods for shape optimization, Springer Berlin Heidelberg (2008) 79–108doi:10.1007/978-3-540-72153-6_4.

[22] R.-E. Plessix, A review of the adjoint-state method for computing the gradient of a functional with geophysical applications, Geophysical Journal International 167 (2006) 495–503. doi:10.1111/j.1365-246X.2006.02978.x.

[23] S. N. Skinner, H. Zare-Behtash, State-of-the-art in aerodynamic shape optimisation methods, Applied Soft Computing 62 (2018) 933–962. doi:10.1016/j.asoc.2017.09.030.

[24] W. Lv, F. Yang, C. Yan, D. Zhou, X. Zeng, Subgradient based multiple-starting-point algorithm for non-smooth optimization of analog circuits, Design, Automation & Test in Europe Conference & Exhibition (2017) 1195–1200doi:10.23919/DATE.2017.7927170.

[25] R. L. Haupt, S. E. Haupt, Practical genetic algorithms, 2nd ed., John Wiley & Sons Inc. (2004) .

[26] A. P. McCabe, G. A. Aggidis, M. B. Widden, Optimizing the shape of a surge-pitch wave energy collector using a genetic algorithm, Renewable Energy 35 (2010) 2767–2775. doi:10.1016/j.renene.2010.04.029.

[27] A. P. McCabe, Constrained optimization of the shape of a wave energy collector by genetic algorithm, Renewable Energy 51 (2013) 274–284. doi:10.1016/j.renene.2012.09.054.

[28] A. Garcia-Teruel, D. I. M. Forehand, Optimal wave energy converter geometry for different modes of motion, Advances in Renewable Energies Offshore: Proceedings of the 3rd International Conference on Renewable Energies Offshore (2018) 299–305.

[29] A. Babarit, A. Clément, Shape optimization of the SEAREV wave energy converter, Proceedings of the 9th World Renewable Energy Congress (2006) .

[30] G. S. Payne, R. Pascal, G. Vaillant, On the concept of sloped motion for free-floating wave energy converters, Proceedings of the Royal Society A: Mathematical, Physical and Engineering Sciences 471 (2015) . doi:10.1098/rspa.2015.0238.

[31] M. López, V. Ramos, P. Rosa-Santos, F. Taveira-Pinto, Effects of the PTO inclination on the performance of the CECO wave energy converter, Marine Structures 61 (2018) 452–466. doi:10.1016/j.marstruc.2018.06.016.

[32] C.-H. Lee, J. N. Newman, Computation of wave effects using the panel method, WIT Transactions on State-of-the-art in Science and Engineering 18 (2005) 211–251. doi:10.2495/978-1-85312-837-0/06.

[33] C.-H. Lee, J. N. Newman, F. G. Nielsen, Wave interactions with an oscillating water column., Proceedings of the Sixth International Offshore and Polar Engineering Conference (1996) 82–90.

[34] O. M. Faltinsen, Sea loads on ships and offshore structures, Cambridge University Press (1990) .

[35] A. J. Chipperfield, P. J. Fleming, The matlab genetic algorithm toolbox, IEE Colloquium on Applied Control Techniques Using MATLAB (1995) doi:10.1049/ic:19950061.

[36] G. S. Payne, Numerical modelling of a sloped wave energy device (2006, accessed on 04/06/20).
URL https://www.era.lib.ed.ac.uk/handle/1842/15607

[37] J. N. Newman, Marine hydrodynamics, The MIT Press (1977) .

[38] H. D. Maniar, A three dimensional higher order panel method based on B-splines (1995, accessed on 04/06/20).
URL http://hdl.handle.net/1721.1/11127